SSRG International Journal of Electrical and Electronics Engineering
ISSN: 2348-8379/ https://doi.org/10.14445/23488379/IJEEE-V13I8P106

Volume 13 Issue 8, 56-69, August 2026

Original Article

An Adaptive Fuzzy Based Grid Forming Inverter Integrated with Hybrid Renewable Source and Storage Unit for Grid Support

Pulidhindi Nagamuneendra[1], K.H.Phani Shree[2]

[1,2]*Department of Electrical and Electronics Engineering, JNTUH University College of Engineering Science and Technology, Hyderabad, Telangana, India.*

[1]*Corresponding Author : muneendra.pulidhindi@gmail.com*

Received: 19 May 2026 Revised: 16 June 2026 Accepted: 23 July 2026 Published: 25 August 2026

***Abstract** - In the modern electrical power systems, the incorporation of renewable energy sources into weak grids has led to power fluctuations, voltage instability, frequency deviations and harmonic distortion. The Grid Forming (GFM) inverters place vital role in a weak grid with low rating and disruptive voltages. The GFM inverter ensures stable voltages magnitudes and frequency of the grid system, which stabilizes the loads connected to the system and injects the required power by the grid, compensating the loads requirement when the grid fails. In this paper, an HRS (Hybrid Renewable Source) and storage unit based GFM inverter is designed for power sharing to the grid. The GFM inverter control includes PQ droop control modules, which define the required voltage magnitude, frequency and phase in synchronization to the grid. The conventional GFM inverter control comprises of PI voltage and current regulators generating the reference signals for the SPWM technique. Due to low damping of the PI regulator, the oscillations and ripple in the signals are increased during initial and transient conditions. This increases the ripple in the DC voltage and injected powers of the renewable source modules. In order to suppress these issues, the PI regulator is replaced with the AFPIC (Adaptive Fuzzy - PI Control) regulator, which ensures increased damping, reducing the ripple. The AFPIC regulator varies the Kp and Ki gains of the PI regulator during the initial and transient states, reducing the disturbances in the reference signals. A relative analysis is presented in this paper with PI and AFPIC regulators integrated into the GFM inverter controller under faulty and transient conditions with the help of MATLAB Simulink software. The results show a significant drop in ripple of DC voltage and renewable injected active powers, THD of the inverter current with the AFPIC regulator, ensuring the robustness of the proposed controller.*

***Keywords** - GFM (Grid Forming), HRS (Hybrid Renewable Source), PQ (Active and Reactive powers), PI (Proportional Integral), SPWM (Sinusoidal Pulse Width Modulation), AFPIC (Adaptive Fuzzy - PI Control), MATLAB Simulink.*

1. Introduction

Penetration of renewable source into the grid for renewable power sharing to the loads is at an increasing pace in modern electrical system. Multiple renewable sources at different locations or combined renewable sources (hybrid) at a single location are the possible structures in the system [1]. In today's technology, most of the renewable sources are solar plants, wind energy systems, biogas plants, tidal energy source etc. The sources have to be connected in parallel to the grid due to unstable power generation from variable natural sources (solar irradiation, wind speed, tides). These sources are connected to a strong grid with a stable voltage and frequency source through an inverter, which is controlled by a grid synchronization controller. With this control module, the complete power from the renewable source is extracted and injected to the grid irrespective of the demand [2]. It has to be ensured that the power requirement is always higher than the renewable power generation for complete power sharing to the grid. However, in weak grid systems with integration of renewables sources to power electronics devices and these are easily affected for small disturbances that led to voltage instability, frequency deviation, distortion in current and low quality of power [3]. This weak grid needs a stable renewable source system which can meet the load demand.

1.1. Literature Review

Grid Following Inverters (GFL) follows the grid voltage and frequency, current changes according to load demand. Due to low short circuit ratio, GFL inverters are more unstable, and power quality is also very poor, but in GFM inverters establish own grid voltage, frequency and its performance depends on variable operating conditions of renewable sources and sudden load variations [4]. Most of the standalone microgrid systems, which include renewable sources, need not have complex control modules as no grid synchronization is needed [5]. [6] Nagasridhar Arise et al. (2023). Introduced a standalone renewable power based micro grid system supporting AC loads [6].

Conventional methods are easy to implement but fails to operate under transient and different loading conditions. [7] Li Lei et al. (2018) proposed a droop controller which gives better results at steady state condition but it is not suggestable for sudden variations of loads due to slow dynamic response [7]. Peter Unruh (2020) introduced a Conventional PI controller with fixed gain values, suitable for constant loads, but it is restricted for dynamic behavior of the system [8]. Ayush K (2023) proposed Fuzzy logic based control method, which gives best results for steady and dynamic loads. A fuzzy logic is ruled-based controller cannot give better results for transient conditions [9]. Musa Khan (2024) analyzed the system under transient and faulty conditions; the conventional controllers do not give efficient operation, and also due to solar irradiance and variable wind speed, both sources can generate low-quality power [10]. Based on the investigation, the following problems identified are voltage instability, frequency deviations, renewable source output power ripples and harmonic distortion in current under transient and fault conditions.

However, the survey reveals a research gap, indicating that limited research is done for integration of renewable sources with intelligent controllers. Most of the research is done with dual renewable sources only. With the Droop controller, Convention PI and fuzzy-based controllers does not gives quality of power, stable DC voltage and constant frequency, and these controllers are not giving stable operation under transient and faulty conditions. To address the research gap and overcome the issues associated with conventional controllers, this paper proposes a novel Adaptive Fuzzy PI Control (AFPIC) regulator is proposed.

This AFPIC regulator is continuously monitor the system, then generates inverter pulses accordingly, which will improve all the system parameters (power ripples, frequency deviation, voltage stability, settling time). The proposed regulator operates effectively under transient and faulty conditions, ensuring the robustness of the regulator. The proposed regulator introduces a four module that creates novelty and reliability of system with more stable parameters for conditions created in the system.

The research includes a wind farm, a PV source and battery module for power generation and management. For grid interconnection of all these sources through a grid synchronization control with feedback from grid voltages is discussed in [11]. The voltage magnitude controls the reactive powers, and the frequency controls the active power. For better control over the grid-tied inverter adaptive fuzzy-based PI regulator is introduced for stable power regulation [12].

In this paper, a stable HRS system with storage backup is connected to the grid through an inverter controlled by a GFM controller [13]. Four renewables are integrated in order to get a more reliable system and enhancing system capacity compared to dual source integration. This GFM control ensures the power sharing to the system meets the load demand, reducing the dependency on the conventional grid source. The GFM control of the inverter makes the weak grid system stable even during sudden load variations. The HRS include PV plant, wind farm, Fuel cell plant and BESS (Battery Energy Storage System) module as the storage backup unit. At the common DC bus, these units are put together, which accumulates the power and shares to the grid through a 6-switch VSI (Voltage Source Inverter).

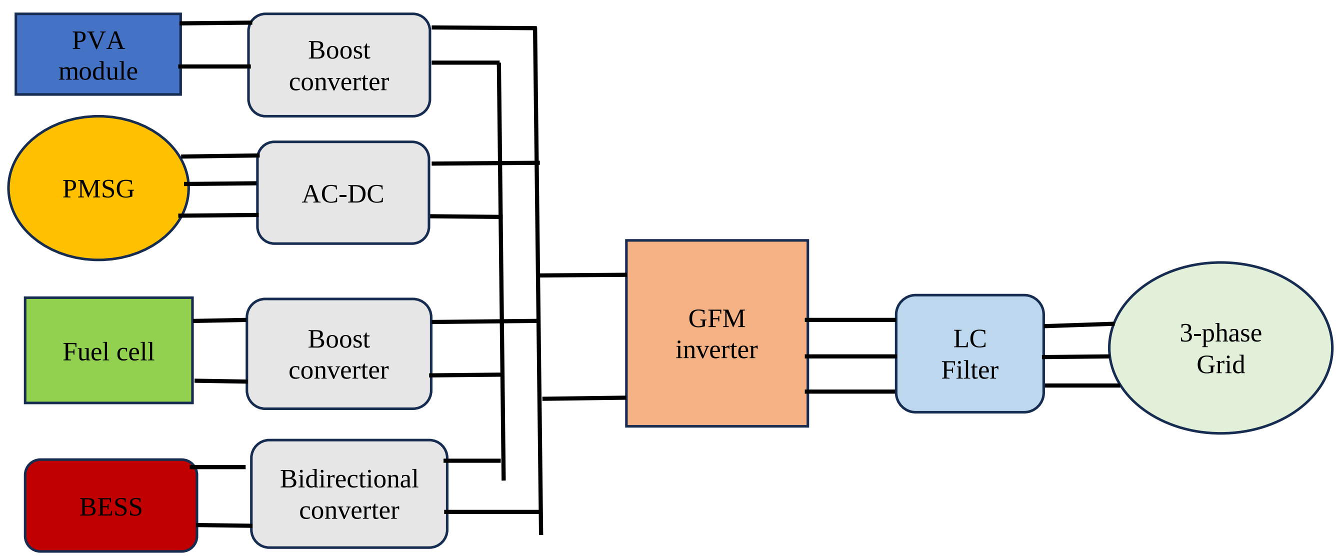

Fig. 1 Proposed HRS grid-connected system

The complete structure of the proposed HRS with storage unit and GFM inverter interconnection to the grid is presented in Figure 1. As illustrated in Figure 1, each renewable and storage module is connected to an individual converter extracting maximum power from the sources at boosted voltage levels. The PVA and Fuel cell module included a boost converter circuit; the windfarm unit included a PMSG (Permanent Magnet Synchronous Generator) connected to a DBR (Diode Bridge Rectifier) and a buck-boost converter for AC-DC conversion. Only the BESS module has a bidirectional DC-DC converter, which enables the controlling charging or discharging of the battery as per the power availability [14]. All the output terminals of the DC-DC converter are connected to a DC bus, which shares the accumulated power to the 3-phase inverter. The inverter is connected to the grid through an LC filter for harmonic filtration caused by the inverter. A load is connected between the HRS system and the grid, consuming power from renewable sources or the grid [15]. In conventional systems, the 3-phase inverter is controlled by the Synchronous Reference Frame (SRF) method, which ensures grid synchronization. However, the SRF method cannot control the active power injection, making it to extract complete power from the battery storage even during excess renewable power conditions. The energy management by the SRF method is not possible as it lacks PQ droop control of the inverter. The PQ droop control, as per the load demand and renewable power availability, can be achieved by GFM control.

Table 1. Characteristics comparison of regulators

Characteristic	Conventional PI	Proposed AFPIC
Gains	Fixed	Variable with respect to error signal
Robustness	Moderately robust	Highly robust to disturbances
Response time	Slower	Faster
Damping	Low damping	Critically damped
Types of system	Only for linear systems	Both linear and non-linear systems
Adaptability	Not adaptable	Adaptive to the changes in the system
Overshoot	High overshoots	Medium overshoots

The GFM control takes feedback from the 3-phase voltages and currents after the inverter LC filter in order to generate reference signals for the PWM generator. The GFM initially is modelled with PI regulator power and current control loops for the generation of reference signals [16]. Due to the drawbacks of the PI regulator (lower damping, slower response time, initial peaks), it is replaced with the AFPIC regulator in the current loops of the GFM controller [17]. This improves the performance of the controller, reducing the disturbances and increase in damping, leading to better voltage and power generation of the modules. The novelty of the AFPIC regulator is addressed by a characteristic comparative Table 1.

This paper is arranged with a proposed outline of the HRS system with a storage unit inter connection to the grid through the GFM inverter in section 1. The internal structure of each renewable module and the storage module is configured in section 2. Section 3 includes the configuration of the GFM control for controlling the 6-switch inverter and the modeling of the AFPIC regulator. The comparative analysis between the regular PI regulator and the AFPIC regulator is presented in section 4, where voltages and powers of all the modules are compared. The determination of the better regulator is validated with a comparison table, and the paper is concluded in section 5, followed by references cited in this paper.

2. System Configuration

In reference of Figure 1, the HRS system comprises of two uncontrolled renewable sources (PV plant and wind farm), one controlled renewable source (Fuel cell) and one storage unit (BESS) [18]. The PV plant and wind farm are considered to be the most penetrable renewable sources, which have higher efficiency and power generation capability using natural sources (solar irradiation and winds). The fuel cell is considered for emergency conditions, which support the grid during higher load demand. The BESS, however, is the backup during deficit power from the renewable sources. It can store excess power during normal operating conditions, which can be utilized later during heavy load conditions. The PV plant is the placement of multiple solar panels in different combinations of series and parallel strings for achieving the desired voltage and power levels [19]. The wind farm is a PMSG-based source which can generate power independently with no external excitation system. The uncontrolled AC output from the PMSG is converted to DC by the DBR. The complete circuit structure of the proposed HRS with storage unit in illustrated in Figure 2. For designing four sources HRS unit, the basic mathematical equations are considered [2,14].

PVA module output current:

$$I = I_{ph} - I_s\left[e\left[\frac{q(V+IRs)}{A_k T}\right] - 1\right] - \frac{V+IRs}{R_{sh}} \qquad (1)$$

Power Ppv= Vpv*Ipv

Where Iph =photo current, Rs & Rsh are resistances.

Mechanical output power for a wind turbine:

$$Pwt = \frac{1}{2}\rho A C_p(\lambda, \beta) V_w^3 \qquad (2)$$

Where λ= Tip speed ratio and β= Blade pitch angle
A=Swept blade area, $\rho =$ Air density, Cp= Power coefficient.

Fuel cell Output voltage with current reference:

$$V_{fc}= E-V_{act}-V_{ohmic}-V_{conc} \quad (3)$$

V_{conc}= concentration loss in volts, V_{act} = activation loss in volts.

Battery output voltage:

$$V_{bat} = E_o - K\,\frac{Q}{Q-iT} + A\,e^{-Bit} - iR \quad (4)$$

Eo= Constant battery voltage, K= Polarization constant, Q= Battery capacity, i= Battery current.

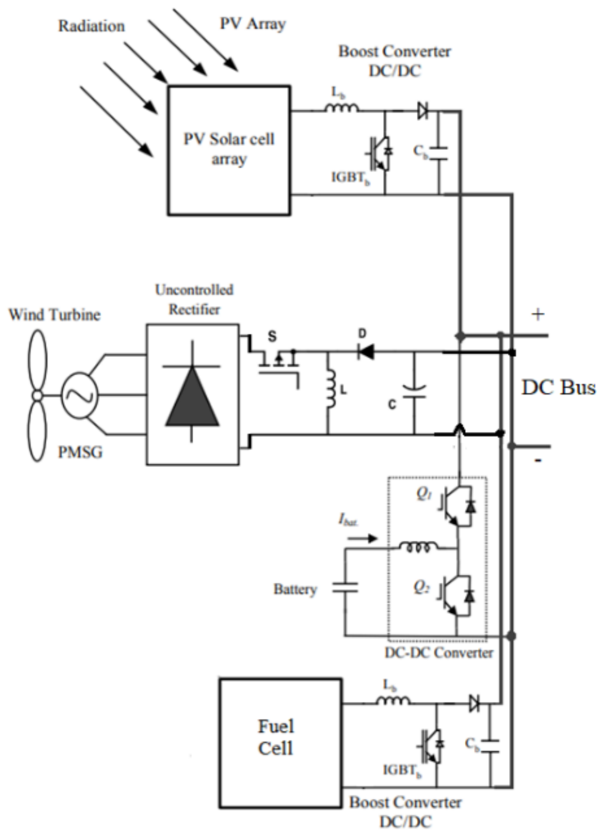

Fig. 2 Circuit structure of the HRS with storage unit

Based on previous research, the PV array and the fuel cell are associated with a Boost Converter (BC) and the wind farm is associated with a Buck-Boost Converter (BBC).

The low voltages of the PV array and the fuel cell are increased by the BC, whereas the rectified PMSG voltage having wide voltage range, which is controlled by the BBC [20]. The uncontrolled renewable source converter switches are controlled by the P&O MPPT (Maximum Power Point Tracking) technique for full power extraction [21]. Whereas the BESS and fuel cell modules are connected with a constant voltage controller with a PI voltage regulator. The constant voltage controller ensures the DC bus voltage is steady at the desired required voltage set by the user. Figure 3 represents the flow chart of P&O MPPT flow chart.

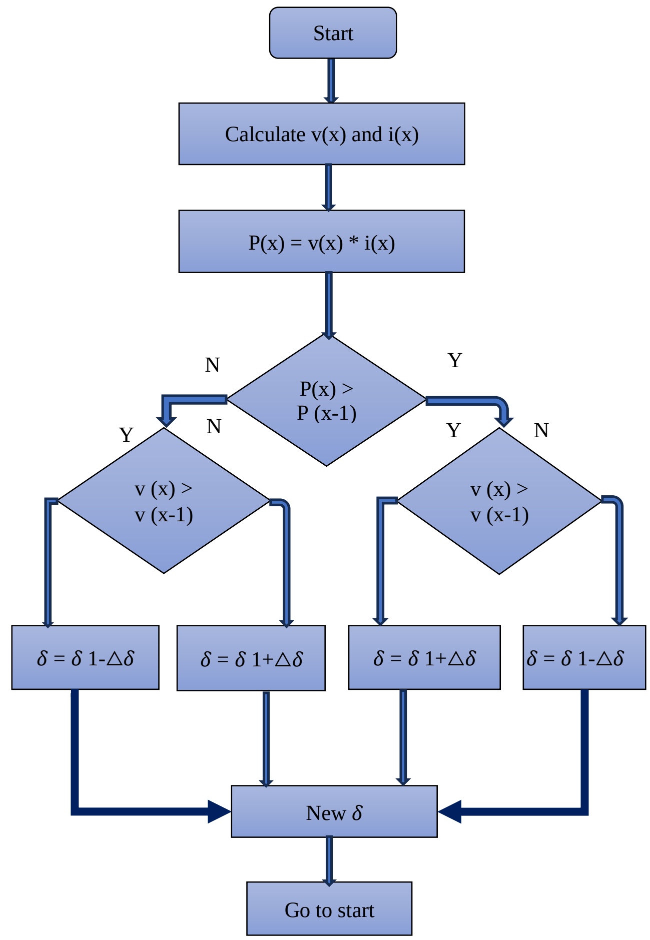

Fig. 3 P&O MPPT flowchart

As mentioned in Figure 3, the duty ratio of the BC switch of the PV module or the BBC switch of wind farm module is controlled by PV module voltage and current, or DBR output voltage or current [22]. The new δ (duty ratio) for the switches is given as

$$\delta = \delta_1 + \Delta\delta; \quad \begin{Bmatrix} If\ P(x) > P(x-1)\ and\ V(x) > V(x-1) \\ If\ P(x) < P(x-1) and\ V(x) < V(x-1) \end{Bmatrix} \quad (5)$$

$$\delta = \delta_1 - \Delta\delta; \quad \begin{Bmatrix} If\ P(x) > P(x-1)\ and\ V(x) < V(x-1) \\ If\ P(x) < P(x-1) and\ V(x) > V(x-1) \end{Bmatrix} \quad (6)$$

Here, V(x) and P(x) are the present values, V(x-1) and P(x-1) are the previous values of voltage and power. δ_1 is the previous duty ratio, and $\Delta\delta$ is either increasing or decreasing value formed by integration of a constant value [23].

The constant voltage controller for the BESS and Fuel cell modules is presented in Figure 4.

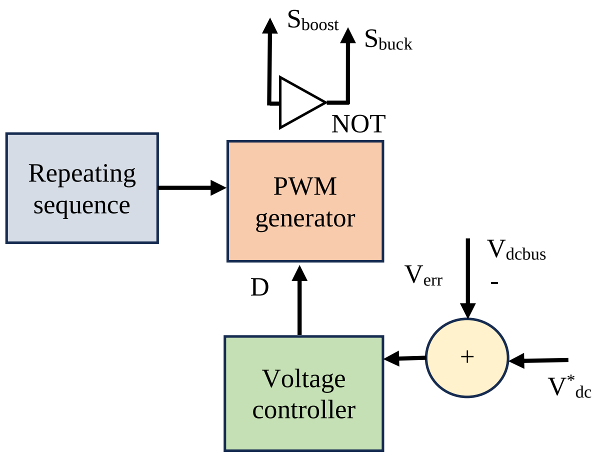

Fig. 4 Constant voltage controller

In the illustrated Figure 4, the controller generates two signals for the two switches (Boost and buck switch) of the bidirectional converter [24]. The duty ratio (D) of the switches is determined by the voltage controller, which is a PI regulator. The duty ratio of the voltage regulator is given as

$$D = (V^*_{dcbus} - V_{dcbus})\left(K_p + \frac{K_i}{s}\right) \quad (7)$$

3. GFM Inverter Design

The GFM inverter in the proposed system includes 6-IGBT switches converting DC voltage to 3-phase two-level voltages at the output. In order to achieve this SPWM technique is used, which needs sinusoidal reference waveforms for the generation of pulses to the IGBT switches [24]. The reference signals are generated using PQ droop control with voltage and current feedback at the output of the LC filter [20]. The control structure of the GFM with PQ droop control is presented in Figure 5.

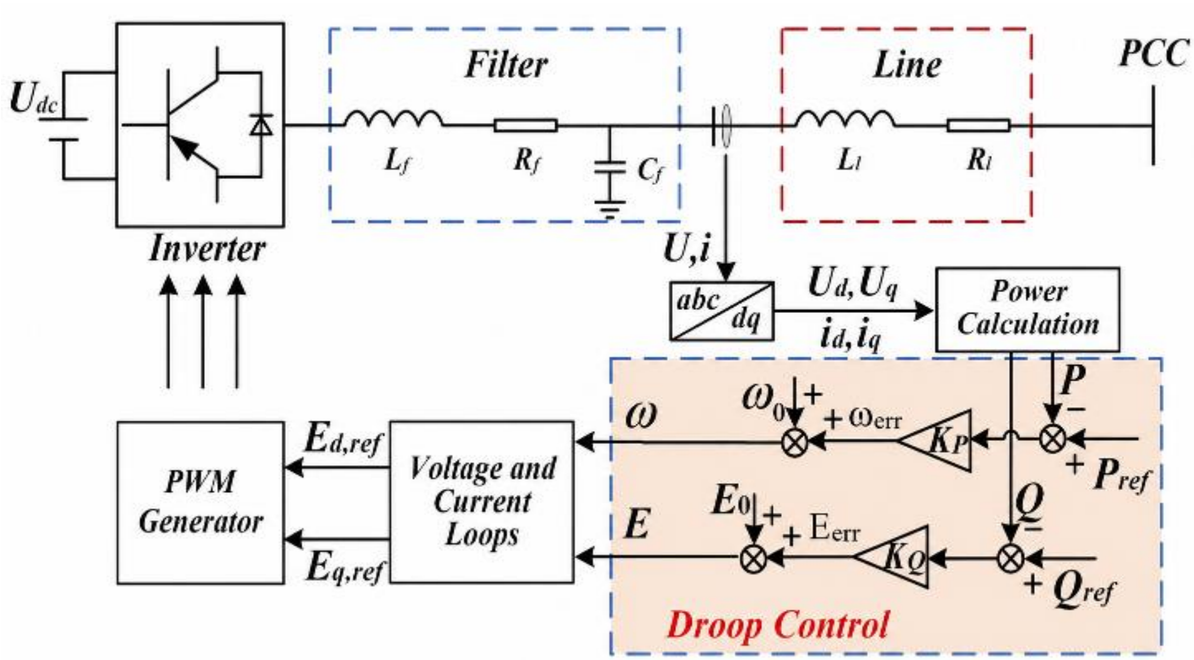

Fig. 5 GFM control with PQ droop controller

Initially, in the GFM control, the active and reactive powers (PQ) are calculated using Park's transformation dq components of the 3-phase voltages and current at the LC filter output [21]. The Park's transformation of the 3-phase signals is given as

$$\begin{bmatrix} X_d \\ X_q \end{bmatrix} = \begin{bmatrix} Sin\,wt & -Cos(wt) & 0 \\ Cos\,wt & Sin(wt) & 0 \end{bmatrix} \begin{bmatrix} X_a \\ X_b \\ X_c \end{bmatrix} \quad (8)$$

In the given Equation (8), the variable 'X' can be either a measured voltage or a current signal. The above Park's transformation expression is considered when the rotating frame is behind 90 degrees to the phase of A.

The 'wt' is the phase angle of A at the LC filter output, which is determined by the PLL block [24]. The powers (PQ) from the dq component of the voltages and currents are calculated as

$$P = \frac{3}{2}(U_d I_d + U_q I_q) \quad (9)$$

$$Q = \frac{3}{2}(U_q I_d - U_d I_q) \quad (10)$$

The measured active and reactive power signals are compared to reference power signals (P_{ref} and Q_{ref}), generating power errors [25]. The error signals are converted to 'Voltage magnitude error' (E_{err}) and 'angular frequency error' (ω_{err}) components by K_P and K_Q gains.

$$\omega_{err} = K_P\left(P_{ref} - P\right) \tag{11}$$

$$E_{err} = K_Q\left(Q_{ref} - Q\right) \tag{12}$$

These error components are added to the per-unit voltage magnitude (E_0) and per-unit angular frequency (ω_0) values, which are considered as '1' for both variables. The updated reference. These reference values are considered in Voltage and Current (V&I) loops for generating the reference dq component of the Sinusoidal signal for inverter control [26].

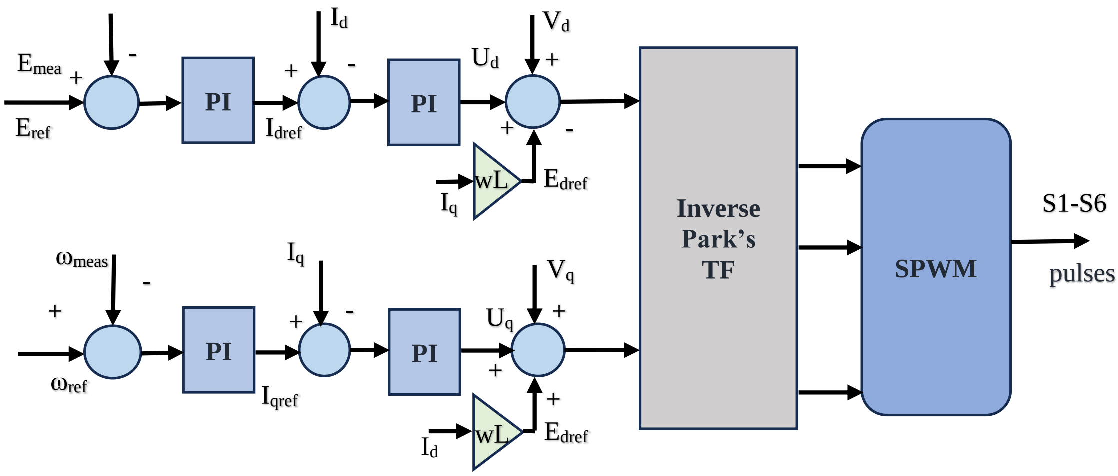

Fig. 6 Internal design of V&I loops

The internal design of the V&I loops of the GFM control is presented in Figure 6. The updated reference voltage error and frequency error components (E_{ref} *and* ω_{ref}) are given as

$$E_{ref} = E_{err} + E_0 \tag{13}$$

$$\omega_{ref} = \omega_{err} + \omega_0 \tag{14}$$

With the reference components E_{ref} *and* ω_{ref} the measured voltage magnitude and angular frequency are measured in per-unit representation. The reference and measured components are compared, generating error signals given to PI regulators. The PI regulator with specific K_p and K_i gains generated reference current dq components given as

$$I_{qref} = \left(\omega_{ref} - \omega_{meas}\right)\left(K_p + \frac{K_i}{s}\right) \tag{15}$$

$$I_{dref} = \left(E_{ref} - E_{meas}\right)\left(K_p + \frac{K_i}{s}\right) \tag{16}$$

The I_{dref} and I_{qref} are compared to i_d and i_q components generated by Equation (4), and the error is given to second loop current PI regulators. The reference voltage components are given as

$$U_d = \left(i_{dref} - i_d\right)\left(K_p + \frac{K_i}{s}\right) \tag{17}$$

$$U_q = \left(i_{qref} - i_q\right)\left(K_p + \frac{K_i}{s}\right) \tag{18}$$

With these dq voltage components calculated, the measured dq voltage components and the loss components, the final dq reference signals are generated as

$$E_{dref} = V_d + U_d - I_q wL \tag{19}$$

$$E_{qref} = V_q + U_q + I_d wL \tag{20}$$

These final reference dq voltage signals are transformed to Sinusoidal abc signals with the help of Inverse Park's transformation, given as

$$\begin{bmatrix} E_{refa} \\ E_{refb} \\ E_{refc} \end{bmatrix} = \begin{bmatrix} Sin\ wt & Cos\ wt \\ Sin\left(wt - \frac{2\pi}{3}\right) & Cos\left(wt - \frac{2\pi}{3}\right) \\ Sin\left(wt + \frac{2\pi}{3}\right) & Cos\left(wt + \frac{2\pi}{3}\right) \end{bmatrix} \begin{bmatrix} E_{dref} \\ E_{qref} \end{bmatrix} \tag{21}$$

Comparing abc reference waveforms to high frequency repeating Sequence Triangular Waveform (SPWM), and then pulses are generated to the inverter switches (S1-S6) [27]. In previous research, the GFM control is not included with advanced adaptive regulators, which results in low damping leading to higher peak overshoots, ripple and disturbances in the parameters. The current and voltage regulators included in the control need to be replaced with more advanced regulators to mitigate these issues. For further enhancement of the GFM control the current PI regulators are replaced with AFPIC regulators, improving the performance of the inverter.

3.1. AFPIC Regulator Design

The AFPIC regulator design is adopted from [28], which is used as a speed regulator for speed control of an induction motor. The regulator performance is tested for different load conditions on the machine. However, the application has no complex controller which need synchronization to another source. The AFPIC regulator is considered to be an advancement to the conventional PI regulator, as the K_p and K_i gains are varied with respect to the error signal. The current regulators, which are connected in the V&I loops of the GFM control, are replaced by the AFPIC regulator [28]. The internal structure of the AFPIC regulator is presented in Figure 7.

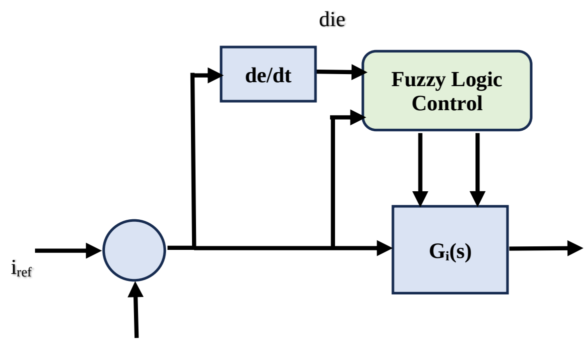

Fig. 7 AFPIC regulator

The AFPIC regulator generates two values, which are the 'change in proportional gain' (Δk_p) and 'change in integral gain' (Δk_i). These values are considered to be output variables of the Fuzzy controller, which vary as per the input values given to the Fuzzy logic. The input variables are considered to be the current error (i_e) and the derivative of current error (di_e) [29]. These error signals can be of d or q axis current components of the current loop in the GFM control. The current PI regulator K_p and K_i gains are varied by the Fuzzy logic output values, which is represented as

$$G_i(s) = (K_p + \Delta k_p) + \left(\frac{K_i + \Delta k_i}{s}\right) \quad (22)$$

Here, K_p and K_i are fixed values, as per the Δk_p and Δk_i values the PI controller gains are changed. Each input variable is set with '7' Membership Functions (MFs), which are arranged in a certain range as per the given input value. There are many types of shapes of MFs in Fuzzy logic, in which the 'triangular' shape is considered to be more precise and faster response. The MFs of the input and output variables (i_e, di_e, Δk_p and Δk_i) defined as per the location in a certain range is presented in Figure 8.

As observed in the Figure 8, the ranges of each variable are different, which are defined as per the requirement of the plant [29]. The 'i_e' is set in the range of '-2 to 2' taken as per the maximum change in the current value in per unit. The 'di_e' variable is set in the range of '-1 to 1', Δk_p from '-0.1 to 0.1' and Δk_i from '-0.01 to 0.01'. The output variable ranges are changed as per the reaction of the controller for the given conditions of the system. The output values of the variables are generated as per the rules linked between the input variables MFs [30]. The rule table for the proposed AFPIC regulator is given in Table 2.

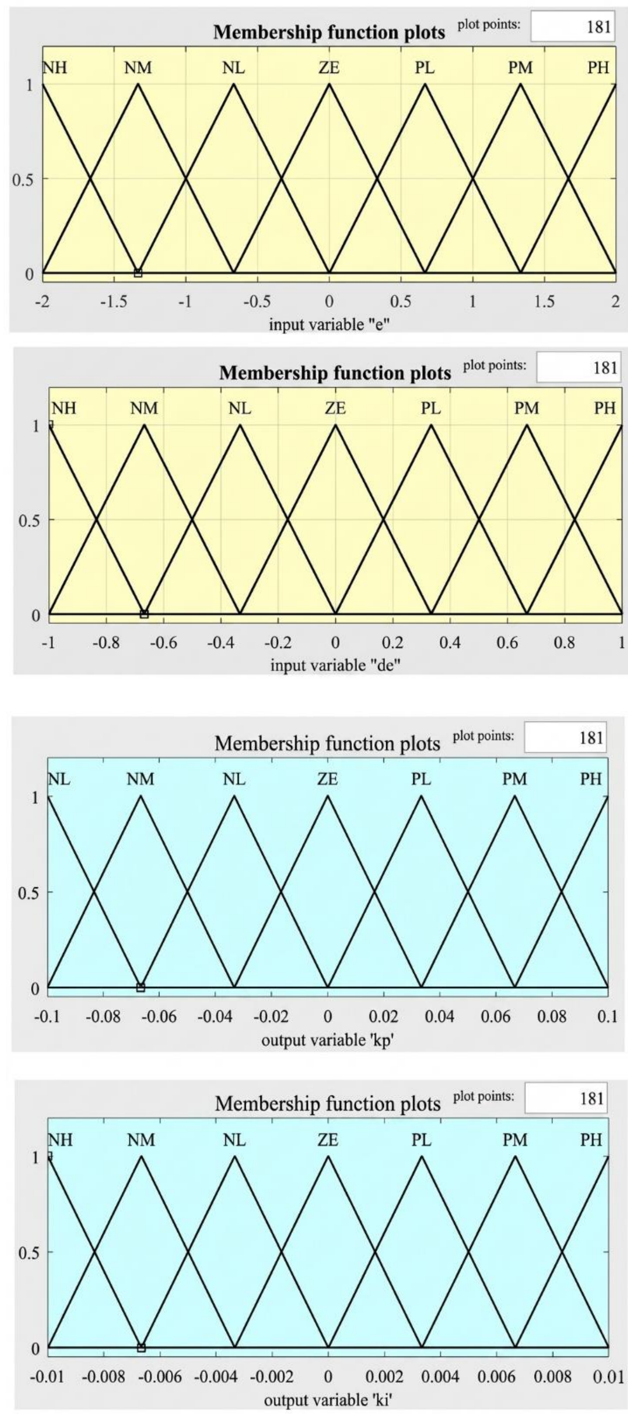

Fig. 8 MFs of input and output variable (i_e, di_e, Δk_p and Δk_i)

Table 2. Rule table

$\Delta k_p \mid \Delta k_i$		i_e						
		NH	**NM**	**NL**	**ZE**	**PL**	**PM**	**PH**
di_e	**NH**	PH|NH	PH|NH	PM|NM	PM|NM	PL|NL	ZE|ZE	ZE|ZE
	NM	PH|NH	PH|NH	PM|NM	PL|NL	PL|NL	ZE|ZE	NL|ZE
	NL	PM|NH	PM|NM	PM|NL	PL|NL	ZE|ZE	NL|PL	NL|PL
	ZE	PM|NM	PM|NM	PL|NL	ZE|ZE	NL|PL	NM|PM	NM|PM
	PL	PL|NM	PL|NL	ZE|ZE	NL|PL	NL|PL	NM|PM	NM|PH
	PM	PL|ZE	ZE|ZE	NL|PL	NM|PM	NM|PM	NM|PH	NH|PH
	PH	ZE|ZE	ZE|ZE	NL|PL	NM|PM	NM|PM	NM|PH	NH|PH

4. Results and Discussion

The modeling of the proposed HRS with a storage unit grid-connected system using GFM controlled inverter is designed in the MATLAB Simulink environment. Blocks from the 'Electrical' subset of the Simulink library are used for the circuit modeling using 'Active and Passive' elements. Two different models are designed with PI regulators and AFPIC regulators for comparative analysis. Both models maintain the same ratings of the renewable and storage modules, which are presented in system configuration Table 3.

Table 3. System configuration

Name of the module	Parameters
Grid	100MVA, 11kV, 50Hz
PV plant	Manufacturer: Sunpreme SNPM-GX-240, Vmp = 33.3V, Voc = 42V, Imp = 7.2A, Isc = 7.8A, Ns = 8, Np = 8, Ppv = 15kW, Boost converter: R_{boost} = 5mΩ, L_{boost} = 1mH, Cin = 100µF, fs = 5kHz
Wind farm	PMSG: 12.5kW, Tm = 70.2Nm, Nrated = 1700rpm, Vdc = 560V. Turbine: Base wind speed = 12m/s, base rotational speed = 1.2pu, pitch = 0.05deg. Buck-Boost converter: Lbb = 0.1mH, Cin = 1mF, fs = 5kHz
BESS	Vnom = 250V, Capacity = 100Ah Bidirectional converter: Lbi = 161.95µH, Co = 220µF, fs = 5kHz, Kp = 0.05, Ki = 0.0023
Fuel cell unit	Vnom = 312V, Inom = 35A, Vend = 215V, Iend = 160A Boost converter: Lb = 1mH, Cin = 100µF, fs = 5kHz, Kp = 0.0035, Ki = 0.0023
GFM inverter	Kp = Kq = 50, E0 = 1, w0 = 1, Kp = 0.05, Ki = 0.01, Kpc = 0.1, Kic = 0.02, fs = 5kHz, Rf = 0.05Ω, Lf = 300µH, Cf = 5KVAR, Transformer: 100KVA, 11KV/260V 50Hz

With the given parameter in Table 3, the simulation is run for 1sec initially with stable values of irradiation and wind speed. The GFM controller Pref and Qref are set with 70kW and 0kVAR values, respectively, to only inject active power from the renewable sources.

Reactive compensation needs to be avoided from the renewable source as they don't generate reactive power as per the rating of the modules; the powers are shared to the grid through the GFM inverter. The battery control reference voltage is set to 500V, and the Fuel cell power reference power is set to 10kW, which calculates 20A reference current for the current regulator.

In the simulation time of 1s the load varied from 30kW to 50kW at 0.5sec to observe the changes in the power of the modules. The powers of all the renewable sources, storage unit, grid and load are presented in Figure 9. As presented in Figure 9, the PV plant and wind farm constantly inject 14.5kW and 9.5kW, respectively, due to stable irradiation and wind speed. As per the given reference current of 20A in the fuel cell unit, the power delivered is 10kW by the fuel cell plant. As the reference set in the GFM inverter control is 70kW, the total renewable power is accumulated to be 34kW, the remaining 36kW is delivered by the battery.

As it can be seen in the graph, the battery is delivering 40kW, the excess 4kW is the power loss of all the sources and the inverter. The load power increases from 30kW to 50kW at 0.5sec, whereas the remaining power delivered tothe grid is dropped from 38kW to 18kW due to increase of load.

The 2kW difference observed in the grid power is the transmission line and transformer loss. For any given condition, the magnitude of voltage and the frequency at the PCC are maintained stable and constant with no much disturbance due to sudden load variation. The magnitude of voltage and frequency at the PCC is presented in Figure 10.

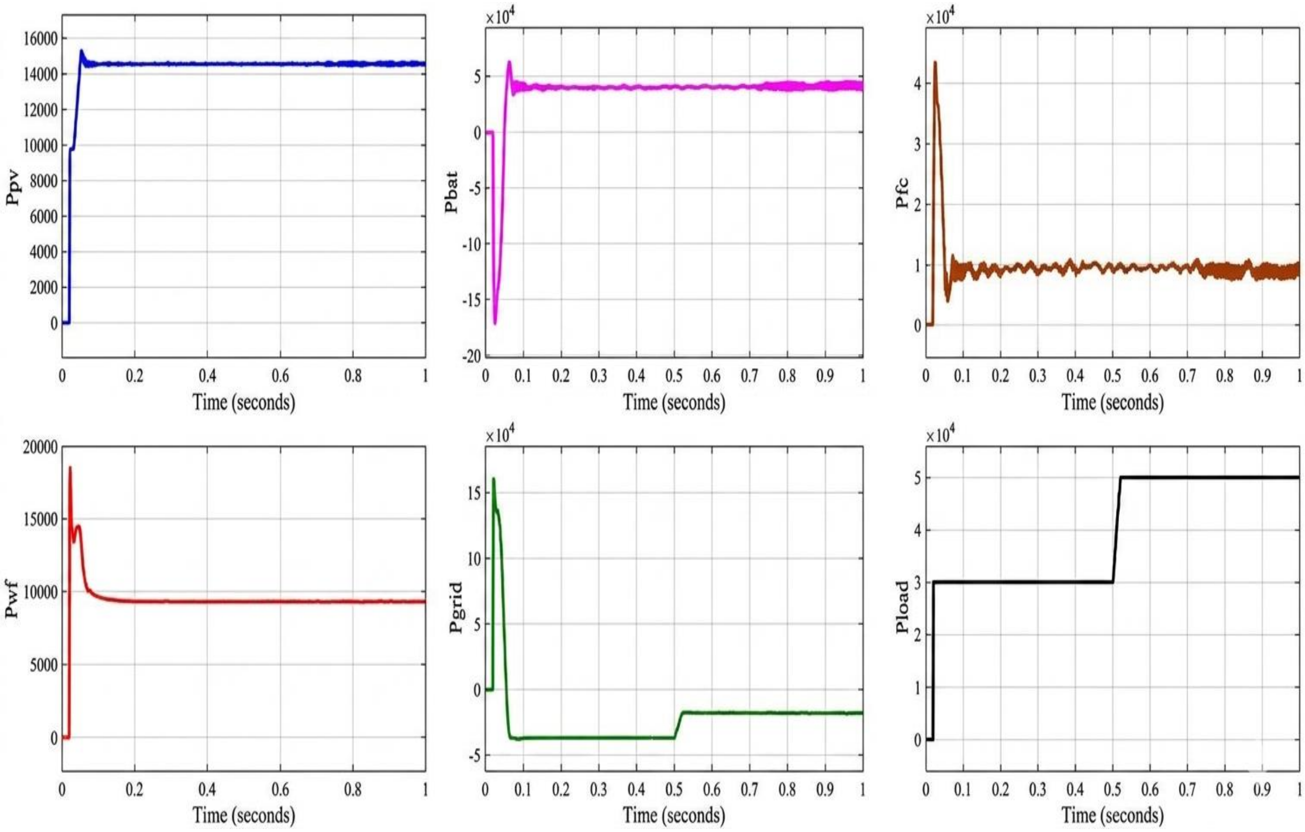

Fig. 9 Powers of all modules connected to the system with the AFPIC regulator

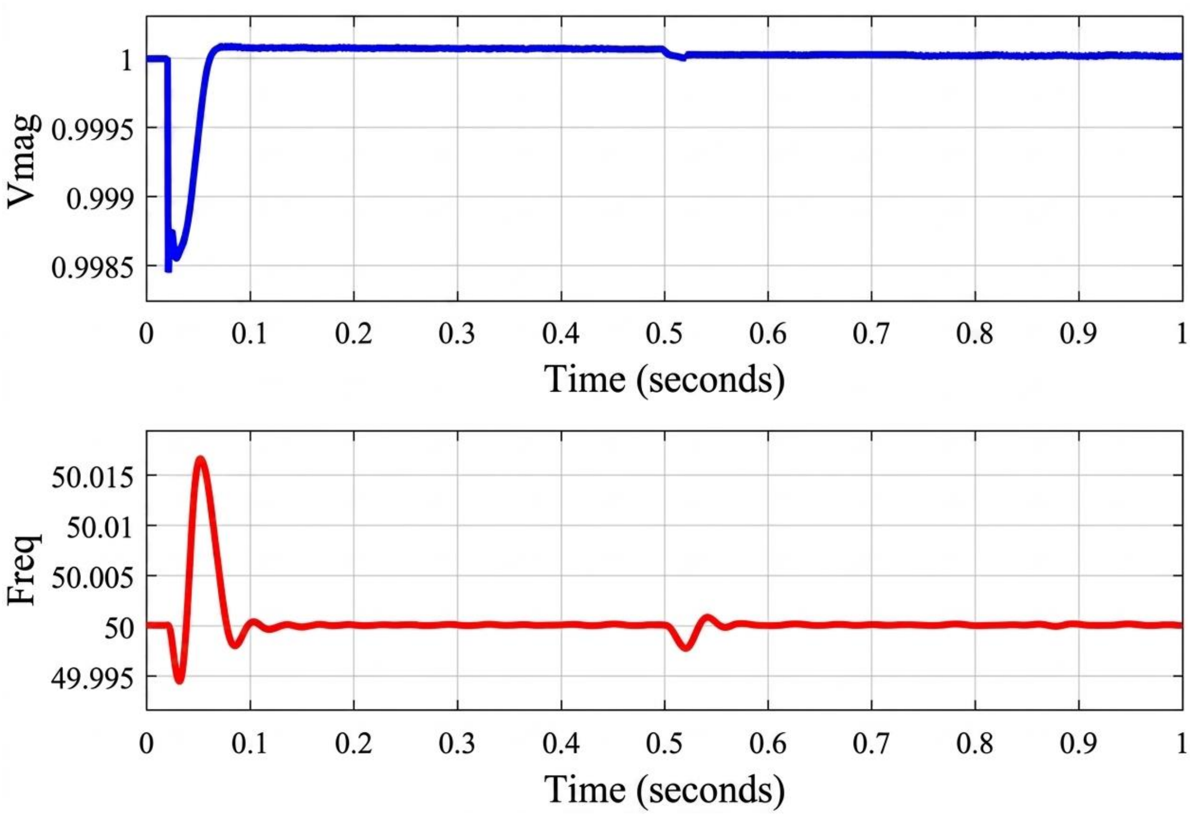

Fig. 10 Magnitude of voltage (pu) and frequency at PCC

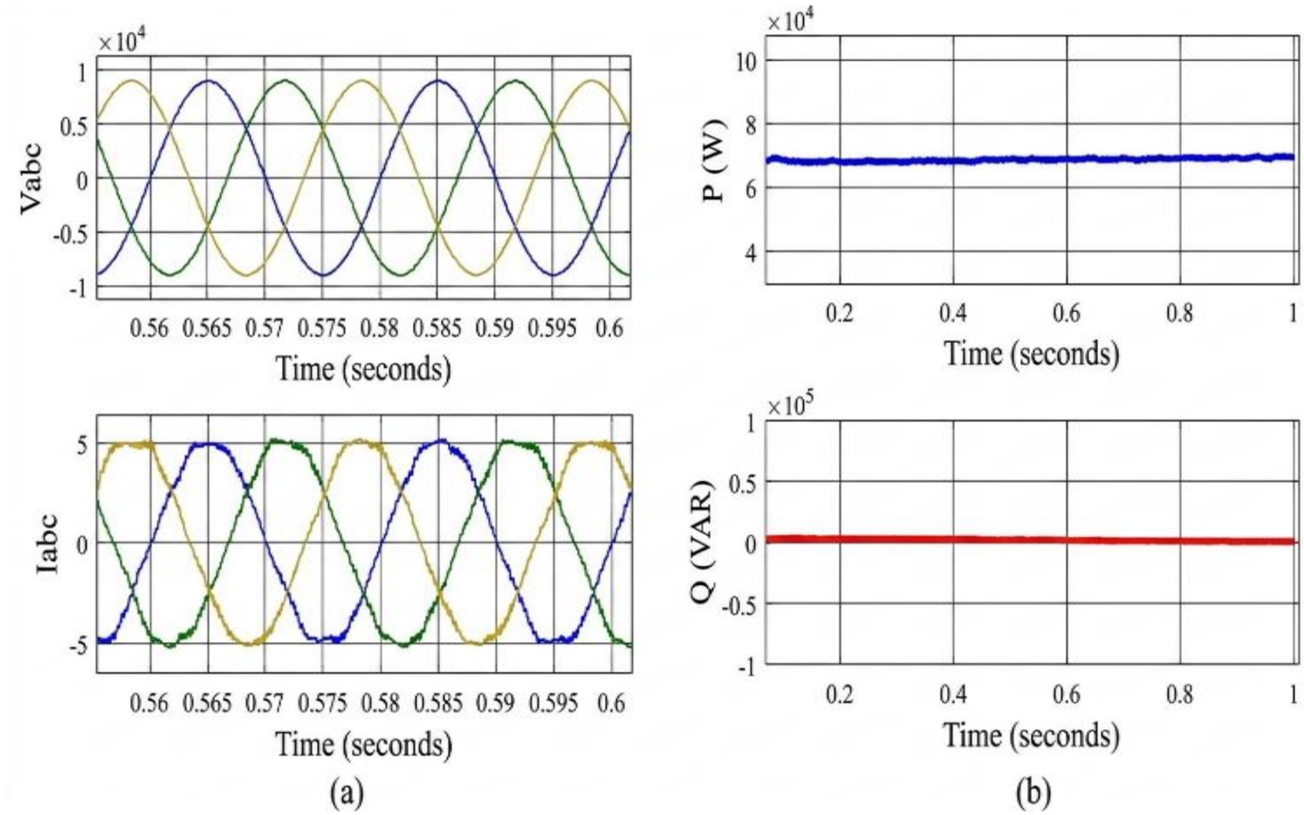

Fig. 11 Measurements after the step-up transformer, (a) 3-ph voltages and current, (b) Active and reactive power.

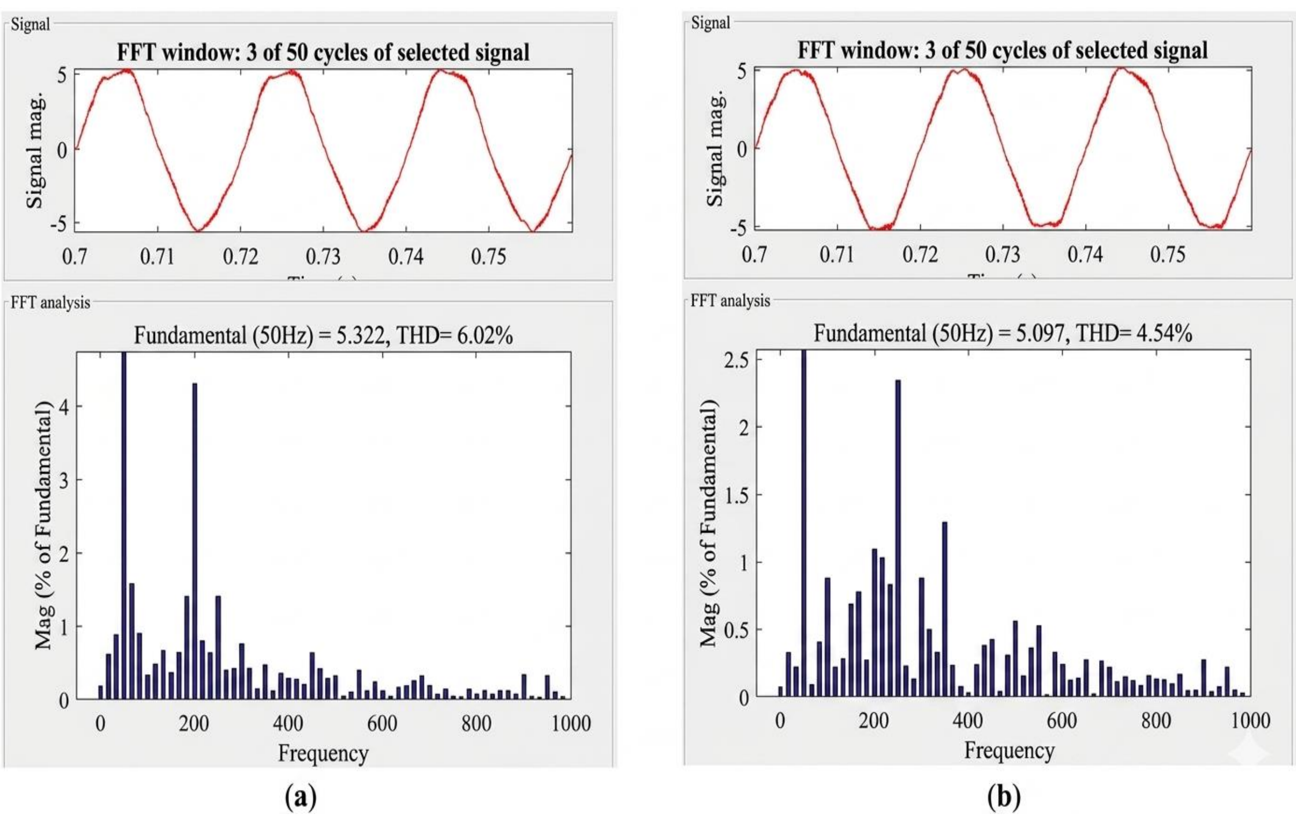

Fig. 12 THD of the injected current (a) PI regulator (b) AFPIC regulator

The 3-phase voltages and the current after the step-up transformer is presented in Figure 11(a), showing a pure Sinusoidal waveform for the voltages. Figure 11(b) presents the total active and reactive power (P&Q) injected through the transformer, recorded to be 70kW and 0VAR to the grid as per the reference set in the GFM controller. The injected current has harmonic content, which his however, in the limit as per IEEE 519-2022 standard. The THD comparison of the injected current with PI and AFPIC regulators is presented in Figure 12. Along with the injected current THD comparison, the ripple of all the shared powers of the sources and the DC bus voltage are also compared, and the graphs are presented in figures below.

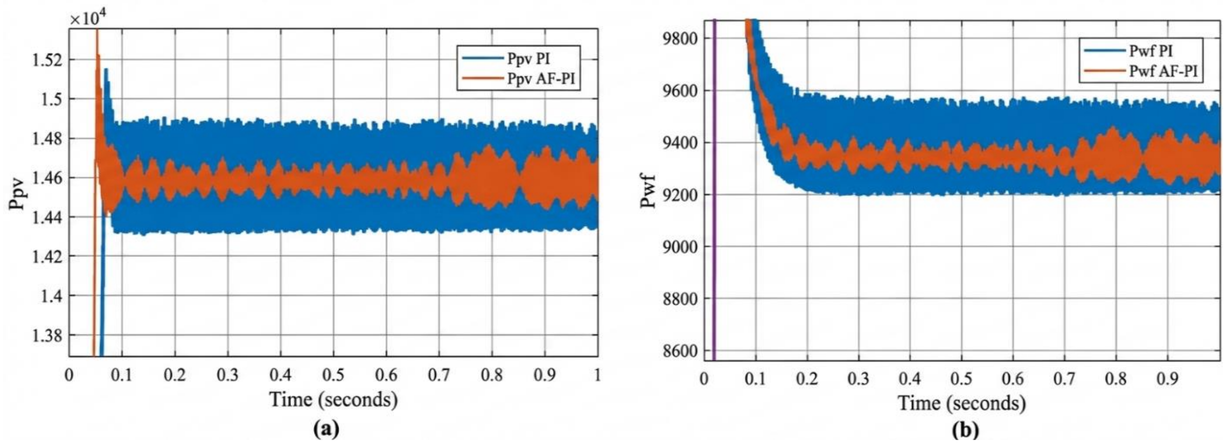

Fig. 13 Active powers of uncontrolled renewable sources, (a) PV plant power (b) Wind farm power.

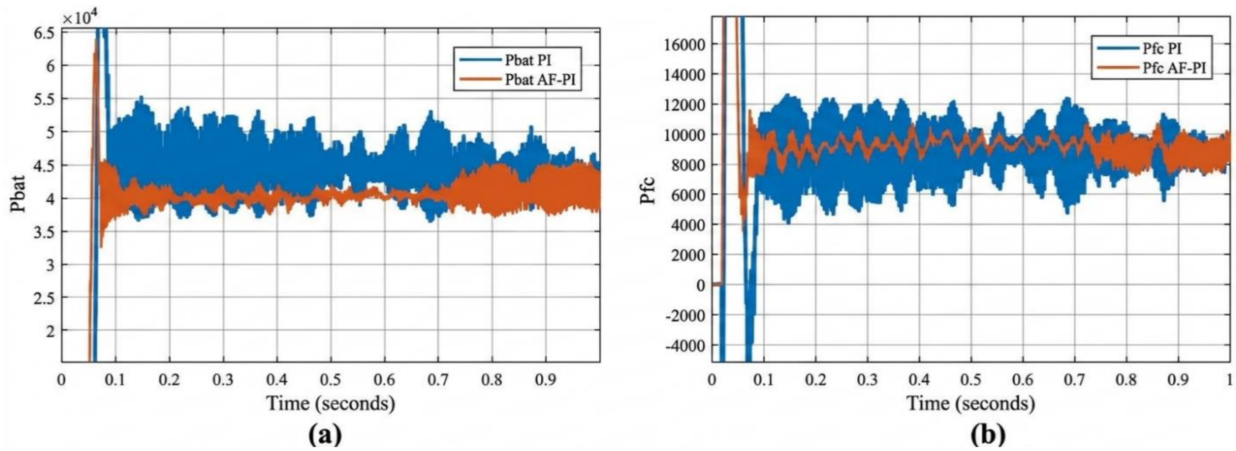

Fig. 14 Active powers of, (a) Storage unit (b) Fuel cell plant.

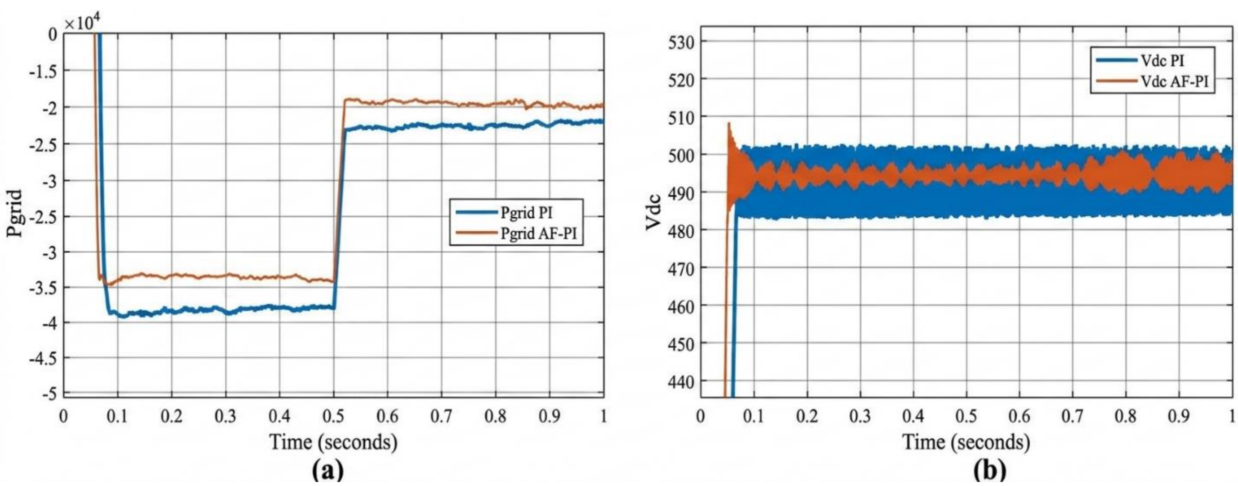

Fig. 15 (a) Active power of grid, and (b) DC link voltage.

In all the power comparison graphs of renewable sources, battery, grid and DC bus voltage in Figures 13(a), and (b), 14 (a), and (b) and 15 (a), and (b), it is observed that the ripple of the powers and voltage are reduced when the inverter is operated with the AFPIC regulator. A ripple percentage and THD comparison Table 4 is given below to validated the updated model.

Table 4. Parametric comparison table

Name of parameter	Conventional PI	Proposed AFPIC
Ppv ripple %	4.1%	2.73%
Pwf ripple %	4.2%	2.1%
Pbat ripple %	36.5%	16.8%
Pfc ripple %	66%	22.2%
Vdc ripple %	3.6%	2%
Vdc settling time	0.07s	0.05s
THD of current	6.02%	4.54%
Power Quality	Low	Improved

In further analysis of the system, the grid side is introduced with an intense fault for a small instant of time at 0.6sec. The fault is three-phase to ground (3P2G), and time is 2 cycles of the fundamental frequency calculated to be 0.04sec. The same fault is introduced in PI and AFPIC regulator models, and comparison are graphs are presented.

As observed in Figure 16, the DC link voltage is not much effected as the fault introduced on the grid side is affects the grid power, which is compensated by the battery power to maintain the DC link voltage and powers of renewable sources stable.

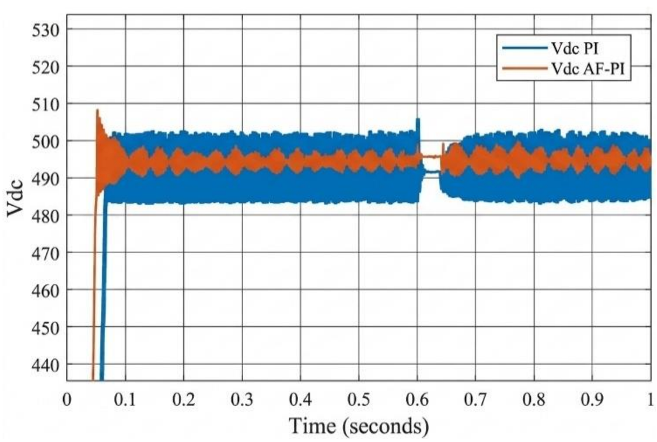

Fig. 16 DC link voltage with 3P2G fault

As presented in Figure 17(a) and 17(b), the active powers of the PV source and wind farm not much effect by the fault. However, the fuel cell power Figure 17(c) drops to near to zero and recovers back after the fault. The battery power drastically changes, and the power injection to the grid is completely reduced to zero during the fault condition, as presented in Figure 17(d) and 17(e).

This shows the robustness of the proposed AFPIC regulator for instantaneous faults, which has the capability to recover and also protect the renewable source from the grid side faults.

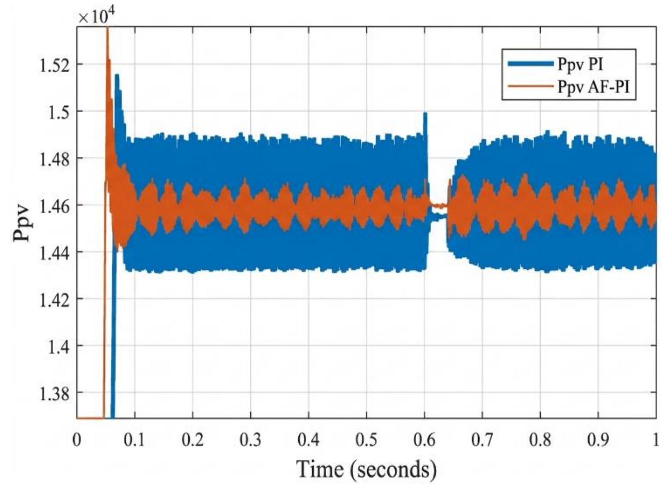

(a)

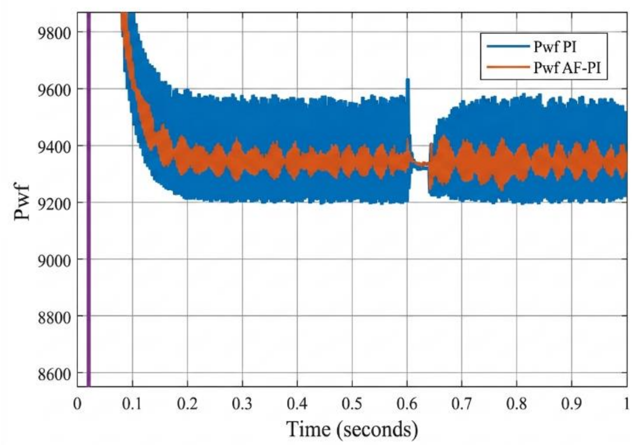

(b)

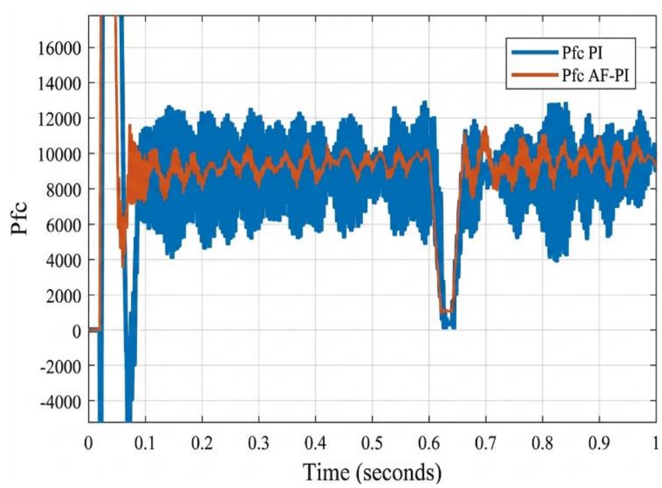

(c)

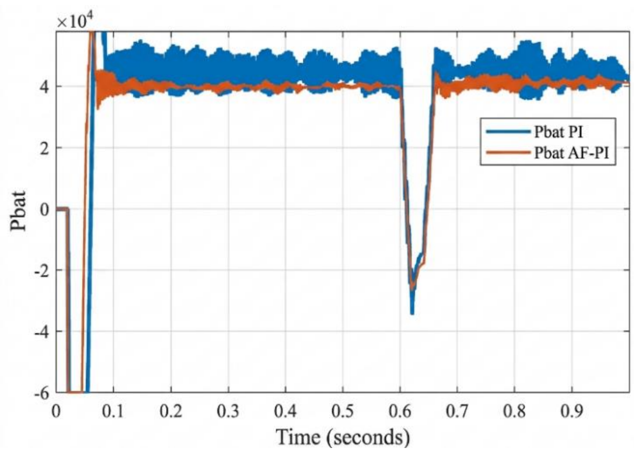

(d)

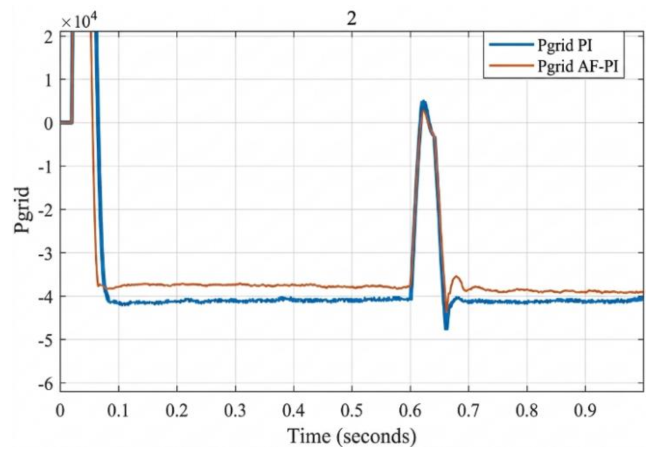

(e)

Fig. 17 Active powers of, (a) PV source, (b) Wind farm, (c) Fuel cell, (d) BESS, and (e) Grid.

5. Conclusion

The performance of the proposed HRS with storage module interconnection to the grid through GFM controlled inverter is analyzed using MATLAB software. The power from uncontrollable renewable sources is maximum extracted, which is either stored in a battery module of delivered to the grid. The controlled renewable source delivers power as per the reference set with respect to the requirement. All the powers from the renewable sources and the battery are delivered to the grid through the inverter controlled by GFM control.

The GFM control initially modelled with a PI regulator, power and current loops are updated with AFPIC current regulators. When the current regulators are replaced, the ripple of the active power delivered by the sources and the DC bus voltage are drastically reduced to half. The settling time of DC bus voltage is also reduced by 0.02sec and the THD of the injected current in reduced from 6.02% to 4.54%, which is below the standardization limit.

The proposed AFPIC regulator efficiently reduces the active power ripple, DC voltage ripple, inverter current THD and also during fault conditions, the system rapidly recovers to a stable operating point, thereby enhancing the robustness of the controller. The GFM inverter performance can further be enhanced by updating the regulators with more advanced intelligent regulators.

Conflicts of Interest

The authors have confirmed that this work has no funding, and there is no conflict of interest.

References

[1] Muhammad Hammad Saeed et al., "A Review on Microgrids' Challenges and Perspectives," *IEEE Access*, vol. 9, pp. 166502-166517, 2021. [CrossRef] [Google Scholar] [Publisher Link]

[2] Anurag Chauhan, and R.P. Saini, "A Review on Integrated Renewable Energy System based Power Generation for Standalone Applications: Configurations, Storage Options, Sizing Methodologies and Control," *Renewable and Sustainable Energy Reviews*, vol. 38, pp. 99-120, 2014. [CrossRef] [Google Scholar] [Publisher Link]

[3] Sara Anttila et al., "Grid Forming Inverters: A Review of the State of the Art of Key Elements for Microgrid Operation," *Energies*, vol. 15, no. 15, pp. 1-30, 2022. [CrossRef] [Google Scholar] [Publisher Link]

[4] Marzie Mirmohammad, and Sahar Pirooz Azad, "Control and Stability of Grid-Forming Inverters: A Comprehensive Review," *Energies*, vol. 17, no. 13, pp. 1-35, 2024. [CrossRef] [Google Scholar] [Publisher Link]

[5] Roberto Rosso et al., "Grid-Forming Converters: Control Approaches, Grid-Synchronization, and Future Trends-a Review," *IEEE Open Journal of Industry Applications*, vol. 2, pp. 93-109, 2021. [CrossRef] [Google Scholar] [Publisher Link]

[6] Nagasridhar Arise et al., "Power Generation of Wind-PV-Battery based Hybrid Energy System for Standalone AC Microgrid Applications," *2023 5th International Conference on Smart Systems and Inventive Technology*, Tirunelveli, India, pp. 261-266, 2023. [CrossRef] [Google Scholar] [Publisher Link]

[7] Li Lei et al., "Power Sharing between Parallel Inverters in Microgrid by Improved Droop Control," *2018 53rd International Universities Power Engineering Conference*, Glasgow, UK, pp. 1-6, 2018. [CrossRef] [Google Scholar] [Publisher Link]

[8] Peter Unruh et al., "Overview on Grid-Forming Inverter Control Methods" *Energies*, vol. 13, no. 10, pp. 1-21, 2020. [CrossRef] [Google Scholar] [Publisher Link]

[9] Ayush K. Varshney, and Vicenç Torra, "Literature Review of the Recent Trends and Applications in Various Fuzzy Rule-based Systems" *International Journal of Fuzzy Systems*, vol. 25, no. 6, pp. 2163-2186, 2023. [CrossRef] [Google Scholar] [Publisher Link]

[10] Musa Khan, Wenchuan Wu, and Li Li, “Grid-Forming Control for Inverter-based Resources in Power Systems: A Review on its Operation, System Stability, and Prospective,” *IET Renewable Power Generation*, vol. 18, no. 6, pp. 887-907, 2024. [CrossRef] [Google Scholar] [Publisher Link]

[11] Qinran Hu et al., “Grid-Forming Inverter Enabled Virtual Power Plants with Inertia Support Capability,” *IEEE Transactions on Smart Grid*, vol. 13, no. 5, pp. 4134-4143, 2022. [CrossRef] [Google Scholar] [Publisher Link]

[12] Sue Wang et al., “Adaptive Fuzzy-based Stability Control and Series Impedance Correction for the Grid-Tied Inverter,” *Mathematical Biosciences and Engineering*, vol. 20, no. 2, pp. 1599-1616, 2023. [CrossRef] [Google Scholar] [Publisher Link]

[13] Habib Ur Rahman Habib et al., “Optimal Planning and EMS Design of PV based Standalone Rural Microgrids,” *IEEE Access*, vol. 9, pp. 32908-32930, 2021. [CrossRef] [Google Scholar] [Publisher Link]

[14] Bhaskara Rao Ravada, Narsa Reddy Tummuru, and Bala Naga Lingaiah Ande, “A Grid-Connected Converter Configuration for the Synergy of Battery-Supercapacitor Hybrid Storage and Renewable Energy Resources,” *IEEE Journal of Emerging and Selected Topics in Industrial Electronics*, vol. 2, no. 3, pp. 334-342, 2021. [CrossRef] [Google Scholar] [Publisher Link]

[15] Shameem Ahmad et al., “A Review of Hybrid Renewable and Sustainable Power Supply System: Unit Sizing, Optimization, Control, and Management,” *Energies*, vol. 17, no. 23, pp. 1-44, 2024. [CrossRef] [Google Scholar] [Publisher Link]

[16] Mohammad Mahdi Rezaei, and Hassan Asadi, “A Modified Perturb-and-Observe-based Maximum Power Point Tracking Technique for Photovoltaic Energy Conversion Systems,” *Journal of Control, Automation and Electrical Systems*, vol. 30, no. 5, pp. 822-831, 2019. [CrossRef] [Google Scholar] [Publisher Link]

[17] Nabil Mohammed et al., “Grid-Forming Inverters: A Comparative Study of Different Control Strategies in Frequency and Time Domains,” *IEEE Open Journal of the Industrial Electronics Society*, vol. 5, pp. 185-214, 2024. [CrossRef] [Google Scholar] [Publisher Link]

[18] Yijing Xie et al., “Virtual Power Plants for Grid Resilience: A Concise Overview of Research and Applications,” *IEEE/CAA Journal of Automatica Sinica*, vol. 11, no. 2, pp. 329-343, 2024. [CrossRef] [Google Scholar] [Publisher Link]

[19] Ouoc Tuan Tran et al., “Stability Assessment of Con Dao Island Grid with High Penetration of Photovoltaic Systems,” *2022 IEEE Power and Energy Society General Meeting*, Denver, CO, USA, pp. 01-05, 2022. [CrossRef] [Google Scholar] [Publisher Link]

[20] Shravani Chapala et al., “Grid Integration of PV-Wind based Hybrid System with UPQC,” *2024 IEEE International Conference on Smart Power Control and Renewable Energy*, Rourkela, India, pp. 1-6, 2024. [CrossRef] [Google Scholar] [Publisher Link]

[21] Seyyed Majid Fatemi, Milad Samady Shadlu, and Amin Talebkhah, “Comparison of Three-Point P&O and Hill Climbing Methods for Maximum Power Point Tracking in PV Systems,” *2019 10th International Power Electronics, Drive Systems and Technologies Conference*, Shiraz, Iran, pp. 764-768, 2019. [CrossRef] [Google Scholar] [Publisher Link]

[22] Jin Cai et al., “Constant-Voltage and Constant-Current Controls of the Inductive Power Transfer System for Electric Vehicles based on Full-Bridge Synchronous Rectification,” *Electronics*, vol. 13, no. 9, pp. 1-20, 2024. [CrossRef] [Google Scholar] [Publisher Link]

[23] Yacine Benatallah et al., “Design and Simulation of the PV Solar System and MPPT with PI Controller based on P&O Algorithm,” *The First National Conference on Renewable Energies and Advanced Electrical Engineering*, pp. 1-4, 2025. [Google Scholar]

[24] Jing Shi et al., “Digital Implementation of Grid-Forming Control for Power Converters using Artificial Delays,” *IEEE/CAA Journal of Automatic Sinica*, vol. 12, no. 11, pp. 2368-2370, 2025. [CrossRef] [Google Scholar] [Publisher Link]

[25] Xue Lyu et al., “Improved Transient Stability Analysis of Multi-Loop Droop-Controlled Grid-Forming Inverters with Current Limiter,” *2024 IEEE Power and Energy Society Innovative Smart Grid Technologies Conference*, Washington, DC, USA, pp. 1-5, 2024. [CrossRef] [Google Scholar] [Publisher Link]

[26] Prakirty Kumari, and Dushyant Sharma, “Performance and Stability Comparison of Grid Forming Inverters with Droop and VSG Controls for Autonomous Microgrids,” *2024 IEEE 11th Power India International Conference*, JAIPUR, India, pp. 1-5, 2024. [CrossRef] [Google Scholar] [Publisher Link]

[27] Mohib Ullah et al., “Dynamic Response of Droop-Controlled Grid-Forming Inverters under Varying Grid for Enhanced Stability in Microgrids,” *Applied Sciences*, vol. 15, no. 23, pp. 1-22, 2025. [CrossRef] [Google Scholar] [Publisher Link]

[28] Hari Maghfiroh et al., “Adaptive Fuzzy-PI for Induction Motor Speed Control,” *Journal of Fuzzy Systems and Control*, vol. 1, no. 1, pp. 1-5, 2023. [CrossRef] [Google Scholar] [Publisher Link]

[29] Wenshao Bu et al., “Improved Adaptive PI-Like Fuzzy Control Strategy of Permanent Magnet Synchronous Motor,” *Energies*, vol. 18, no. 2, pp. 1-16, 2025. [CrossRef] [Google Scholar] [Publisher Link]

[30] Muhammad Waqas Qaisar, and Jingyang Fang, “Grid-Forming Converters for Renewable Generation: A Comprehensive Review,” *Energies*, vol. 18, no. 17, pp. 1-25, 2025. [CrossRef] [Google Scholar] [Publisher Link]